Laboratory study of the frictional rheology of sheared till

Andrew P. Rathbun,[1] Chris Marone,[1] Richard B. Alley,[1] and Sridhar Anandakrishnan[1]

[1] Deformation of till produces power law creep for low strain at stresses high enough to cause permanent deformation but below the shear strength. Experiments were conducted on till (a mixed size granular material) from Matanuska Glacier, Alaska, and the Scioto (Ohio) Lobe of the Laurentide Ice Sheet (Caesar till). We deformed till in double direct shear under fixed shear velocity or shear stress (creep). Normal stress ranged from 50 kPa to 5 MPa at shearing rates ranging from 1 to 300 μm/s for 1 cm thick samples. Creep was induced via small step perturbations in stress. Fabric development within till layers was investigated by varying shear strain prior to creep tests. In velocity-controlled experiments, till deforms as a nearly Coulomb plastic material with slight velocity strengthening, corresponding to a stress exponent, $n > 60$. Creep experiments conducted well below the shear strength indicate lower n values, increasing as shear stress increases. With increasing initial strain and inferred fabric development, the creep strain rate decreases while n increases. Experiments at a normal stress of 1 MPa and no initial strain show $n = 6.8$, increasing to $n = 17.5$ at higher shear strains; however, strain rate was still decreasing and thus these values represent maximum estimates. Our data show that in the absence of dilatant hardening till exhibits rate sensitivity at strain of order 1 or less. At low strains, n likely depends on consolidation state, permeability, and dilation. Deformation is nearly rate insensitive (Coulomb plastic) at shear stress near the shear strength or at high strain.

1. Introduction

[2] Glaciers can move by a variety of processes, with deformation of subglacial till playing a major role for some valley glaciers, ice streams, and ice sheets [e.g., *Paterson*, 1994; *Alley*, 2000; *Clarke*, 2005]. Seismic studies have shown that the material under fast-moving ice streams is highly porous water-saturated sediment (till) [*Alley et al.*, 1986; *Blankenship et al.*, 1986; *Peters et al.*, 2006]. The actively deforming layer, which ranges in scale between centimeters and several meters [e.g., *Kamb*, 1991; *Engelhardt and Kamb*, 1998; *Truffer et al.*, 2000], is produced by reworking of sediment or by wear processes such as abrasion or plucking. At high effective stress (overburden stress minus pore water pressure), the shear strength of till is larger than the shearing resistance of ice, so deformation only occurs within the ice; at low effective stress, till is more likely to deform than ice [e.g., *Engelhardt et al.*, 1990; *Paterson*, 1994]. Effective stresses may range from a few kPa or less to a few hundreds of kPa with channelized water drainage favoring higher values [*Alley et al.*, 1989a; *Engelhardt et al.*, 1990; *Paterson*, 1994; *Engelhardt and Kamb*, 1997]. Low effective stress can also limit bed deformation by allowing sliding at the ice-bed interface [e.g., *Kamb*, 2001; *Iverson et al.*, 2003].

[3] Early studies of bed deformation assumed a viscous or near-viscous relation for till deformation [e.g., *Boulton and Hindmarsh*, 1987]. Laboratory tests of till deformation are sparse [e.g., *Tulaczyk*, 2006], but have produced important results leading to the idea that till is more nearly a Coulomb plastic (treiboplastic) material [e.g., *Kamb*, 1991, 2001; *Iverson et al.*, 1997, 1998; *Tulaczyk et al.*, 2000]. However, debate still exists as to whether till is best characterized by a "viscous" rheology (with a nearly linear relation between shear stress and strain rate) or "plastic" rheology (for which shear stress is related to strain rate raised to a power of 10 or more) [e.g., *Kamb*, 1991; *Jenson et al.*, 1995; *Hindmarsh*, 1997; *Iverson et al.*, 1998; *Alley*, 2000; *Tulaczyk et al.*, 2000; *Fowler*, 2003, *Kavanaugh and Clarke*, 2006]. This study aims to couple current ideas on frictional rheology, drawn in part from studies in fault mechanics and granular materials, with those of Coulomb plastic failure and time-dependent viscous creep at stresses below the steady shear strength at high strain.

2. Terminology

[4] Technical terms differ between the various communities that study friction and the rheology of glacial and

---

[1]Rock and Sediment Mechanics Laboratory and Pennsylvania State Ice and Climate Research, Department of Geosciences, Pennsylvania State University, University Park, Pennsylvania, USA.

granular materials. We have chosen what we believe are widely accepted usages, but we define them here for clarity. Our experiments employ either a controlled shear velocity or a controlled shear stress, with measurements of the resulting shear stress or shear velocity, respectively. In either case, we may calculate a bulk shear strain rate for the sample using the measured layer thickness and the boundary offset. If shear stress exceeds the yield strength, permanent deformation occurs. The shear stress value at which the bulk sample undergoes macroscopic and steady frictional shear is referred to as the residual shear strength.

[5] When permanent deformation is occurring, the deformation rate or shear strain rate may increase with shear stress. Data can be modeled by assuming that the strain rate increases as a power, n, of the stress, so this is often called power law creep. The case in which the strain rate increases linearly with stress is linear-viscous deformation. The concept of viscosity is based on a stress exponent of one, but the deformation may (very loosely) be termed viscous for any exponent of the order of 1. To distinguish between true Newtonian viscosity and what we approximate as viscous, we use the term "pseudoviscous".

[6] At some sufficiently high shear stress, it becomes difficult to further raise the stress; the material can undergo arbitrarily rapid deformation. If we neglect further, second-order variations in stress that may arise from changes in strain rate, this strength is called the residual shear strength; related terms in the literature include ultimate, steady state, or fully mobilized strength. The residual shear strength typically exhibits second-order variations with velocity. Shear strength increases (velocity strengthening) or decreases (velocity weakening) with the logarithm of velocity or, alternatively, strain rate varies as a high power of the stress. The case of velocity-independent strength satisfies perfectly plastic behavior, with all shear stresses (friction values) being equal for all shear strain rates assuming a constant effective stress. This case can be modeled as a power law with the exponent tending to infinity and is termed Coulomb plastic or treiboplastic behavior.

[7] Most laboratory studies of till deformation have used a constant velocity boundary condition and evaluated results in the context of a Coulomb plastic model in which shear strength is independent of strain rate and varies linearly with effective normal stress [e.g., Kamb, 1991, 2001; Iverson et al., 1997, 1998; Tulaczyk et al., 2000]. By definition, the Coulomb failure criterion for frictional sliding (and also brittle fracture) is independent of strain rate or sliding velocity. Coulomb's failure criterion is a relationship that describes stresses at failure; it is not a rheology or constitutive law relating stress and strain rate. Coulomb [1781] showed that the residual shear strength during frictional sliding between many types of surfaces varies roughly linearly with normal stress; he found the same relationship holds for the fracture strength or maximum (peak) frictional strength. Although Coulomb failure defines brittle deformation, several investigators have found that it applies to materials undergoing permanent–plastic–deformation [e.g., Kamb, 1991; Iverson et al., 1998; Tulaczyk et al., 2000]. In these cases, the plastic shear strength scales with mean

stress, as predicted by Coulomb's criterion; hence, the usage of Coulomb plastic deformation.

3. Previous Work

[8] Early studies of till deformation focused on rheologies of the form

$$\dot{\gamma} \propto \frac{(\tau - \tau_c)^n}{P_e^m}, \tag{1}$$

where $\dot{\gamma}$ is the strain rate, τ shear stress, τ_c yield stress, and P_e the effective normal stress (normal stress minus pore pressure). For example, Boulton and Hindmarsh [1987] used equation (1) to describe flow of till near the terminus of Breidamerkurjokull in Iceland. They reported values for n and m slightly above 1, these values suggest a slightly nonlinear viscous relation for till. A viscous till model, $n = 1$, has been assumed on a theoretical basis in many studies [e.g., Alley et al., 1989a, 1989b; Hindmarsh, 1997; Fowler, 2003]. The other end-member of equation (1) is $n = \infty$, which belongs to the family of models referred to as plastic deformation models because strain rate variations are extreme for even small changes in shear stress. In the limit, plastic deformation implies that strain rate cannot be predicted directly from shear stress.

[9] Relatively few controlled stress experiments have been conducted on till. Ho et al. [1996] carried out tests on Batestown till from the Lake Michigan Lobe of the Laurentide Ice Sheet, in which shear stress was stepped and the strain rate measured. In their tests, stress was held constant for 24 h, but strain rate decreased with time. This resulted in the stress exponent, n, decreasing with time. Ho et al. [1996] suggested an exponent of $1.3-3.1$ for stresses below the shear strength in both direct shear and triaxial configurations. Kamb [1991] carried out simple constant stress direct shear tests on till from Ice Stream B (now Whillans Ice Stream), Antarctica described by Engelhardt et al. [1990]. Below the shear strength of the till, shear strain rate decreased with time, whereas above the shear strength of the till the shear strain rate increased with time to presumably unrecordable levels. Kamb [1991] concluded that n would be large, approximating Coulomb plastic deformation. Constant shear stress experiments were also conducted in a ring shear device by Moore and Iverson [2002], in which normal stress was reduced until creep occurred. That study showed that shear displacement results in dilation and pore pressure reduction within the deforming layer, limiting rapid shear.

[10] In practice, measurements of residual shear strength are often fitted by a Coulomb-Mohr failure envelope

$$\tau_{res} = c + P_e \tan \phi, \tag{2}$$

where τ_{res} is the residual shear strength, c is cohesion, and ϕ the angle of internal friction. Equation (2) is known to apply in many situations at and near Earth's surface. For example, it describes the strength of tectonic faults in Earth's upper crust.

[11] Experiments have shown that in addition to approximately obeying equation (2), residual shear strength for friction (and other measures of strength) often exhibits
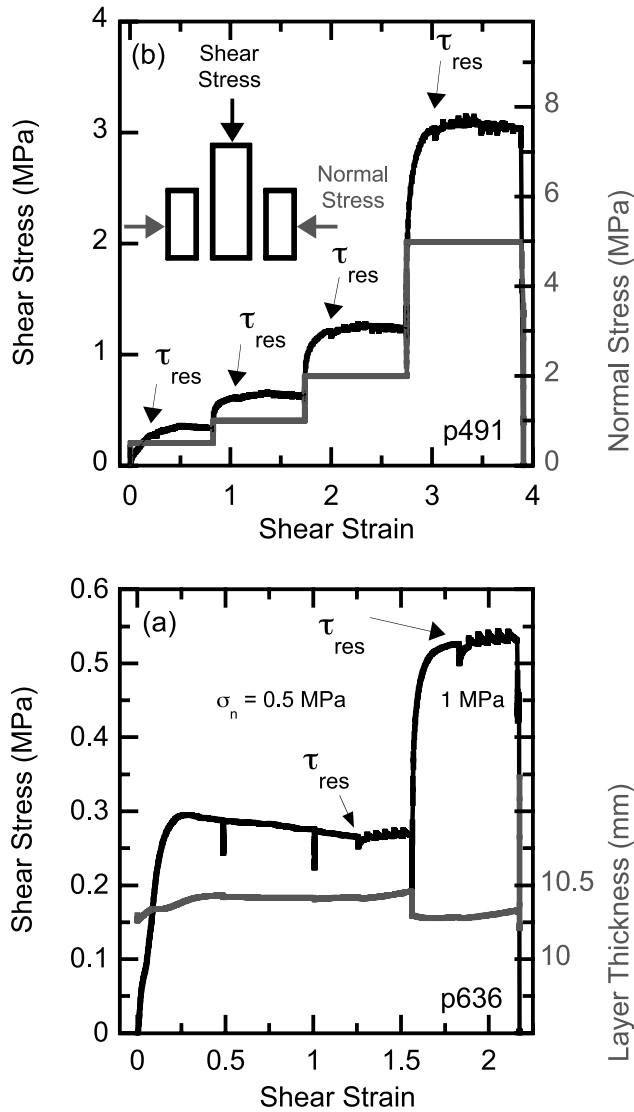
Figure 1. Shear stress plotted as a function of displacement and normal stress. Normal stress is held constant while the sample is sheared at a constant rate of 10 μm/s until a residual shear stress (τ_{res}) value is obtained. The displacement rate is then stepped to investigate frictional properties of till. After completion of velocity steps, normal stress is increased to a new steady value and displacement repeated. (a) Caesar till is displaced to 12.2 mm before velocity steps, showing offsets where the DCDT was reset at 5 and 10 mm. After completion of velocity steps, normal stress is increased and the sample displaced 2.2 mm before velocity steps. Layer thickness evolves to a constant value before τ_{res} is obtained. Because of geometric effects, a constant slope represents a constant layer thickness during shear, and following standard practice this trend is removed [e.g., *Scott et al.*, 1994]. Increases in layer thickness with changes in velocity result from dilation. (b) Matanuska till was displaced 1.6 mm before step increases in velocity. Complete displacement histories for all experiments can be found in Table 1. Inset shows double direct shear geometry with shear stress applied vertically and normal stress horizontally. A grooved steel block is driven between two stationary grooved blocks. The nominal contact area is held constant at 10×10 cm^2, with an initial layer thickness of 1 cm.

small, systematic variations with driving velocity or strain rate. In experiments on till, these results are described in the form

$$\frac{\tau_{res}}{\tau_o} = 1 + B\ln\frac{\dot{\gamma}}{\dot{\gamma}_o}, \tag{3}$$

where τ_o is the steady state shear strength at a reference strain rate $\dot{\gamma}_0$ and τ_{res} is the steady state shear strength at a new strain rate $\dot{\gamma}$. The constant B has been estimated at ~0.01–0.015 from studies on clays [*Skempton*, 1985; *Mitchell and Soga*, 2005]. Many materials exhibit a slight decrease in shear strength with increasing shear velocity, corresponding to a negative value of B. *Iverson et al.* [1998] obtained −0.01 for till from Storglaciaren and −0.010 for Two Rivers till. Equation (3) can be written as a flow law:

$$\dot{\gamma} = \beta\dot{\gamma}_o\exp\left(k\frac{\tau_{res}}{\tau_o}\right), \tag{4}$$

where k is $1/B$ and β is $\exp(-k)$ [*Kamb*, 1991; *Hooke et al.*, 1997]. This form takes τ_{res} as the independent variable and predicts the shear strain rate.

[12] Equation (3) shares features of the rate and state friction laws developed in studies of rock friction and earthquake physics [e.g., *Dieterich*, 1979, 1981; *Ruina*, 1983]. These studies show that friction exhibits small, systematic changes as a function of displacement history (state) and slip velocity (rate) [*Marone*, 1998]. Typically, the steady state coefficient of sliding friction varies with the log of sliding velocity and may increase or decrease with an increase in velocity, which is termed velocity-strengthening or velocity-weakening frictional behavior, respectively. The change in shear stress with velocity in rate and state friction would result in values of n above 60 [*Kamb*, 1991; *Iverson et al.*, 1998; *Tulaczyk et al.*, 2000; this study]. Some form of slip-weakening (decreased friction with increased shear strain) or velocity-weakening is required for stick-slip motion [*Dieterich*, 1979, 1981]. Stick-slip frictional motion is thought to be a good analog for seismic slip [*Brace and Byerlee*, 1966] and perhaps for recently discovered glacial earthquakes in Antarctica [e.g., *Anandakrishnan and Bentley*, 1993] and Greenland [*Ekstrom et al.*, 2003, 2006].

4. Experimental Procedure

4.1. Testing Apparatus

[13] Experiments were conducted in a servocontrolled, double direct shear apparatus at room temperature under either saturated or nominally dry conditions. This apparatus consists of two hydraulic rams, which can be operated in constant velocity loading by displacement feedback or in constant shear stress loading by load feedback. The double direct shear geometry involves two layers of sample sandwiched between three forcing blocks (Figure 1 inset). Forcing blocks are constructed from hardened steel with dimensions of $10 \times 10 \times 2$ cm for the side blocks and $10 \times 15 \times 3$ cm for the center block. Nominal frictional contact area is constant throughout shear at 10×10 cm. Geometric thinning of the layer occurs as a consequence of shear, and layer thickness data are corrected accordingly [e.g., *Scott et al.*, 1994]. The faces in contact with till are grooved

perpendicular to the shear direction to a depth of 0.8 mm and spacing of 1 mm, which ensures that shear occurs within the layer rather that at the till-steel interface [*Anthony and Marone*, 2005; *Knuth and Marone*, 2007]. Further details on the apparatus are given by *Mair and Marone* [1999], *Karner and Marone* [2001], and *Frye and Marone* [2002].

[14] Samples were constructed in a leveling jig by placing a cellophane tape wall around the steel side blocks to 10 ± 0.2 mm above the top of the grooves, then filling the area with till. Precision ground blocks were used to level the till layer before placing the center block. The same procedure was used to construct two layers for each experiment (Figure 1 inset). This produced an initial layer thickness of 10 ± 0.2 mm. Steel guide plates were attached to the unstressed sides of the sample to reduce till loss (Figure 1 inset). To prevent sample loss during shear, thin copper shims and a sheet of latex rubber were applied to the underside of the assembly. The base of each steel block was coated with a thin layer of molybdenum lubricant to reduce friction between the bottom of the side blocks and support blocks and allow sample dilation or compaction.

[15] Water-saturated experiments were conducted on Caesar till samples at room temperature and atmospheric pressure under saturated-drained conditions. In these experiments, a rubber sheet surrounding the block configuration was filled with water. The sample was allowed to equilibrate for 45 min, which was sufficient to completely saturate the layer.

[16] We measured shear and normal displacement and force continuously during all experiments using load cells and Direct Current Displacement Transducers (DCDT) attached to the load point. Experiments were run at constant normal stress, and thus displacements normal to the layer are changes in layer thickness. We measured initial layer thickness under load to an accuracy of ±0.01 mm and corrected these values for the elastic stiffness of the loading frame. Stiffness is 3.7 MN/cm and 5 MN/cm for the horizontal and vertical load frames, respectively. Shear strain within the layer was calculated as engineering shear strain, γ

$$\gamma = \sum_{i=1}^{X_{max}} \frac{x_i - x_{i-1}}{h_i}, \qquad (5)$$

where x_i is the displacement, h is the instantaneous layer thickness at increment i, and X_{max} is the total displacement. Shearing velocity was controlled by updating a servocommand signal at 300 Hz. The control resolution of each ram is 0.1 μm/s in displacement feedback or 0.1 kN in load feedback. All signals were recorded at 16 or 24-bit resolution. Recording rate was kept $\geq$10 samples per micron of shear displacement in rate-controlled experiments. All creep experiments were recorded at a constant 10 Hz. Details of experiment conditions are given in Table 1.

4.2. Sample Characteristics

[17] We collected till from the toe of the Matanuska Glacier, Alaska and the former Scioto Lobe of the Laurentide Ice Sheet in Columbus, Ohio. The latter has been identified as Caesar till and dates to ~19,500 years ago

[*Haefner*, 1999]. All samples were allowed to air-dry, then were disaggregated by hand before grain-size analysis separation. Grain sizes less than 63 μm were analyzed using laser diffraction on a Malvern Mastersizer. Caesar till is well sorted and composed primarily of sand-sized grains whereas Matanuska till is poorly sorted with more silt-sized grains. Details of the grain-size distributions are given in Table 2.

[18] The testing arrangement requires that grains larger than 1 mm are removed to maintain a 10 to 1 ratio of layer thickness to maximum particle size. This ensures that shear is homogeneous, initially, and that a few, large, particles do not dominate stress-strain behavior. This limitation on particle size necessitated removing 57% and 18%, by weight, of the material collected from the Matanuska Glacier and Caesar till, respectively. Past experiments on multiple grain sizes and fractal grain-size distributions [*Marone and Kilgore*, 1993; *Mair and Marone*, 1999] indicate that large particles may affect fabric development, and second-order frictional characteristics; however, bulk rheology and frictional strength is unaffected. Variations in bulk clay mineral content, which may occur with sieving, are likely to have an effect on friction constitutive properties [e.g., *Bird*, 1984; *Logan and Rauenzahn*, 1987; *Iverson et al.*, 1998; *Brown et al.*, 2003; *Ikari et al.*, 2007]; however, most clay mineral grains are much smaller than our 1 mm cutoff size, so we do not expect significant variation via sieving. The effect of particle size on till rheology is an interesting issue and merits study, for example by stepwise removal of coarse particles, however, the present configuration is ill suited for such work.

4.3. Experimental Procedure
4.3.1. Constant Shear Velocity

[19] Experiments run under controlled slip velocity were employed to find the shear strength and rate-dependent strength of till. A normal stress was applied and held constant before the onset of shear. We first determined the steady state shear strength at a constant shear velocity of 10 μm/s and then changed shear velocity to 1, 3, 10, 30, 100, and 300 μm/s to investigate second-order frictional characteristics (Figure 1). Shear strength was measured as a residual value when stress no longer changed with displacement. Velocity steps resulted in small "saw tooth" variations in shear stress (Figure 1) with the first, negative, saw tooth the result of decreasing velocity from 10 to 1 μm/s. After the completion of shear velocity steps, normal stress was increased and the experiment repeated. To check reproducibility and stress history effects, normal stress was held constant or decreased in some experiments (Table 2).

[20] We correct layer thickness data for geometric shear thinning, which occurs during direct shear, using a standard technique [*Scott et al.*, 1994]; our data show initial dilation and steady thickness (porosity) values during shearing (Figure 1a). After the shear strength measurements, the subsequent step increase in shear velocity causes dilation (Figure 1).

[21] The vertical ram is limited to 6 mm increments of displacement in high-resolution mode. After attaining 6 mm of displacement, the motion is stopped for 10–30 s while the vertical DCDT signal is reset. This procedure results in a

Table 1. List of Experiments

Experiment	Normal Stress, MPa	Material[a]	Run-In Length, mm	Loading Boundary Condition[b]
p490s10tr.5	0.5, 1	Matanuska 2B Dry	1.6, 0.4 velocity steps	D; 1, 3, 10, 30, 100, 300
p491s10tr.5	0.5, 1, 2, 5	Matanuska 2B Dry	1.6, 0.4 velocity steps	D; 1, 3, 10, 30, 100, 300
p495s10tr.5	0.5, 1, 2	Matanuska 2D Dry	1.6, 0.4 velocity steps	D; 1, 3, 10, 30, 100, 300
p497s10tr.5	0.5, 1, 2, 5	Matanuska 2B Dry	1.6, 0.4 velocity steps	D; 1, 3, 10, 30, 100, 300
p509s10tr.5	0.5, 1, 2, 5	Matanuska 2B Dry	1.6, 0.4 velocity steps	D; 1, 3, 10, 30, 100, 300
p538s10tr.5	0.5, 1, 2, 5	Matanuska 4C Dry	1.6, 0.4 velocity steps	D; 1, 3, 10, 30, 100, 300
p539s10tr.5	0.5, 1, 2, 5	Matanuska 4C Dry	1.6, 0.4 velocity steps	D; 1, 3, 10, 30, 100, 300
p546s10tr.5	0.5, 1, 2, 5	Matanuska 4C Dry	1.6, 0.4 velocity steps	D; 1, 3, 10, 30, 100, 300
p571s10tr.05	0.053, 0.087, 0.174	Matanuska 4B Dry	1.6	D
p572s10tr.05	0.053, 0.087, 0.174	Matanuska 4B Dry	1.6	D
p584s10tr05	0.5, 1, 2, 5	Caesar Dry	1.6, 0.45 velocity steps	D; 1, 3, 10, 30, 100, 300
p585s10tr005	0.05, 0.1, 0.15, 0.2	Caesar Dry	1.6, 0.45 velocity steps	D; 1, 3, 10, 30, 100, 300
p588s10tr05	0.5, 0.5, 1	Caesar Dry	1.6, 0.45 velocity steps	D; 1, 3, 10, 30, 100, 300
p593s10tr005	0.05, 0.1, 0.15, 0.2	Caesar Dry	2.2, 0.45 velocity steps	D; 1, 3, 10, 30, 100, 300
p601s10tr005	0.05, 0.1, 0.15, 0.2	Caesar Dry	2.2, 0.45 velocity steps	D; 1, 3, 10, 30, 100, 300
p602s10tr005	0.05, 0.05, 0.05	Caesar Dry	2.2, 0.45 velocity steps	D; 1, 3, 10, 30, 100, 300
p603s10tr005	0.2, 0.15, 0.1, 0.05	Caesar Dry	2.2, 0.45 velocity steps	D; 1, 3, 10, 30, 100, 300
p617s10tr05	0.5, 1, 2, 5	Caesar Dry	6.2, 0.45 velocity steps	D; 1, 3, 10, 30, 100, 300
p621s10tr05	0.5, 0.5, 1	Caesar Saturated	7.2, 0.45 velocity steps	D; 1, 3, 10, 30, 100, 300
p622s10tr2	2, 2, 5	Caesar Saturated	7.2, 0.45 velocity steps	D; 1, 3, 10, 30, 100, 300
p624s10tr005	0.05, 0.05, 0.05, 0.1	Caesar Saturated	7.2, 0.45 velocity steps	D; 1, 3, 10, 30, 100, 300
p626s10tr005	0.05	Caesar Saturated	21	D
p627s10tr005	0.05	Caesar Saturated	21	D
p628s10tr005	0.05, 0.1	Caesar Saturated	12.2, 0.45 velocity steps	D; 1, 3, 10, 30, 100, 300
p633s10tr005	0.05, 0.05, 0.1	Caesar Saturated	12.2, 0.45 velocity steps	D; 1, 3, 10, 30, 100, 300
p634s10tr01	0.150, 0.2	Caesar Saturated	12.2, 0.45 velocity steps	D; 1, 3, 10, 30, 100, 300
p635s10tr01	0.2, 0.15	Caesar Saturated	12.2, 0.45 velocity steps	D; 1, 3, 10, 30, 100, 300
p636s10tr05	0.5, 1	Caesar Saturated	12.2, 0.45 velocity steps	D; 1, 3, 10, 30, 100, 300
p638s10tr5	5	Caesar Dry	12.2, 0.45 velocity steps	D; 1, 3, 10, 30, 100, 300
p718s10tr01	1	Caesar Dry	10 run in	S; 2
p719s10tr01	1	Caesar Dry	10 run in	S; 2
p722s10tr01	1	Caesar Saturated	10 run in	S; 2
p724s10tr01	1	Caesar Dry	10 run in	S; 2
p729s10tr01	1	Caesar Saturated	10 run in	S; 2
p731s10tr01	1	Caesar Saturated	10 run in	S; 5
p732s10tr01	1	Caesar Saturated	10 run in	S; 5
p737s10tr01	1	Caesar Saturated	10 run in	S; 2
p746s10tr01	1	Caesar Saturated	10 run in	S; 2
p750s10tr01	1	Caesar Dry	10 run in	S; 5
p757s10tr01	1	Caesar Dry	0	S; 5
p758s10tr01	1	Caesar Saturated	0	S; 2
p760s10tr01	1	Caesar Saturated	0	S; 2
p761s10tr01	1	Caesar Saturated	0	S; 5
p793s10tr01	1	Caesar Saturated	0	S; 5
p797s10tr01	1	Caesar Saturated	0	S; 5
p804s10tr01	1	Caesar Saturated	0	S; 5
p1025s10tr01	1	Caesar Saturated	4.9 run in	S; 5
p1109s10tr01	1	Caesar Saturated	4.8 run in	S; 5
p1125s10tr01	1	Caesar Saturated	1.4 run in	S; 5
p1131s10tr01	1	Caesar Saturated	2.1 run in	S; 5
p1230S10tr5	5	Caesar Saturated	0.9 run in	S; 5
p1231S10tr5	5	Caesar Saturated	0	S; 5
p1253S10tr05	0.5	Caesar Saturated	1.0 run in	S; 5
p1261S10tr05	0.5	Caesar Saturated	0	S; 5

[a]Number and letter combinations indicate sample B, C, or D at location 2 or 4.
[b]Displacement is indicated by D and rates are given in μm/s, and stress is indicated by S and step size is given in % of shear strength.

shear stress drop (vertical curves in Figure 1a) due to creep while the ram is held stationary, but shear stress quickly recovers when shear begins again.

[22] To investigate the second-order rate dependence of strength, we conducted experiments in which the rate of shearing is increased in a series of incremental steps. Shear velocity was varied from 1 to 300 μm/s (Figure 2). A displacement of 400–450 μm at each velocity was sufficient for friction to reach a new steady level; the friction value at each velocity represents the steady state shear strength at that shear velocity. A step increase of velocity

Table 2. Grain-Size Distributions

Material	Bulk Sample	Experimental Range
Matanuska Site 2	94.9% sand, 4.4% silt, 0.8% clay	87.2%, 11.2%, 1.6%
Matanuska Site 4	84.4% sand, 12.7% silt, 2.9% clay	54.8%, 32.7%, 7.5%
Caesar	98.9% sand, 1.0% silt, 0.1% clay	98.7%, 1.2%, 0.1%
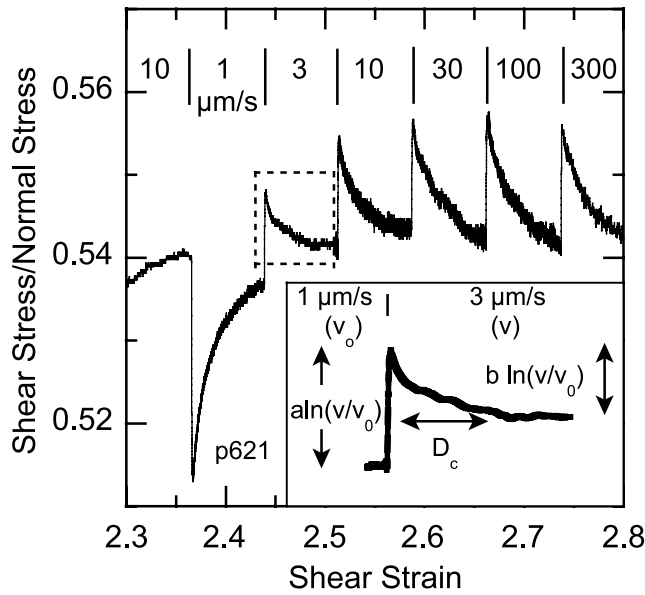
Figure 2. Velocity stepping portion of experiment under controlled shear velocity for Caesar till. An initial displacement at 10 μm/s is followed by a series of steps. Velocity history is given. Inset shows frictional response to a step increase in velocity. When velocity is increased, frictional strength increases instantaneously and then decays over a characteristic sliding distance. In this example, the instantaneous increase is larger than the subsequent decay, and therefore steady state sliding friction increases with increasing velocity.

resulted in a sharp increase in friction of $\sim$0.01 followed by displacement-dependent decay to a new steady level over a characteristic distance. Once steady state friction was reached, a new velocity was imposed and the process repeated. Figure 2 inset presents a single velocity step.

4.3.2. Constant Shear Stress

[23] A series of experiments were conducted under constant shear stress conditions to investigate the time-dependent deformational (or "creep") behavior of Caesar till. Controlling shear stress allowed for a direct measurement of the power law stress exponent, such as employed in some studies of till rheology. Experiments were performed at 0.5, 1, or 5 MPa normal stress and an initial layer thickness of 10 mm. Samples were sheared under both dry and water-saturated conditions. To account for minor variations in residual shear strength between experiments, one can normalize the shear stress value, τ, by the residual shear strength τ_{res} measured in each experiment, and report these normalized stresses τ^*

$$\tau^* = \tau/\tau_{res}. \qquad (6)$$

[24] Our main set of creep experiments began with a shear displacement of 10 mm under controlled shear velocity of 10 μm/s (Figure 3). This provided a measurement of τ_{res}, and produced a consistent shear fabric within the layers. We found that it was important to keep the initial shear strain history identical between experiments, in order

to account for minor variations in inferred fabric and τ_{res}. The boxed regions in Figure 3 represent portions of the experiment conducted in shear displacement control, whereas the central section of the experiment was conducted under controlled shear stress. Figure 3b presents the same experiment as Figure 3a plotted versus shear strain to highlight the displacement-controlled section of the experiment. Figure 3 also illustrates the difference in time and
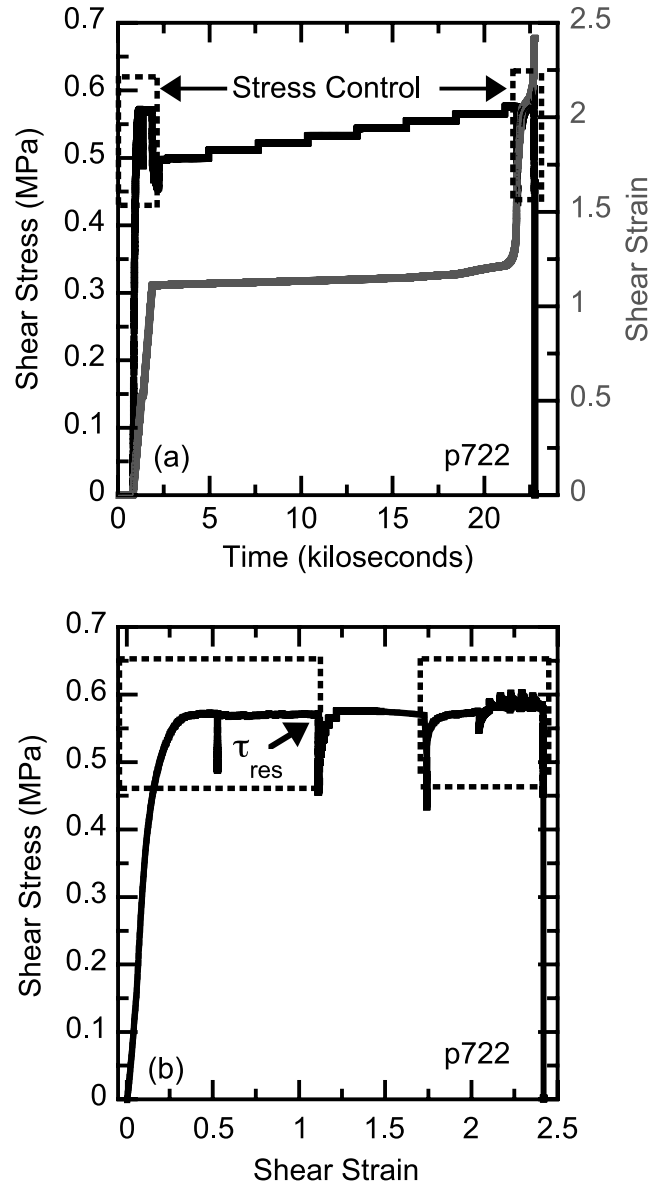
Figure 3. Creep experiments conducted under controlled shear stress. Each experiment involves some deformation in which shear stress is controlled and additional deformation in which shear strain rate is controlled, as indicated by the unboxed and boxed regions, respectively. (a) Experiment plotted against time to highlight stress control. (b) The same experiment plotted against shear strain to highlight the run in. During the initial run in, residual shear strength (τ_{res}) is established. Shear stress is reduced prior to creep tests. After completion of creep tests, shear strain rate is once again controlled.
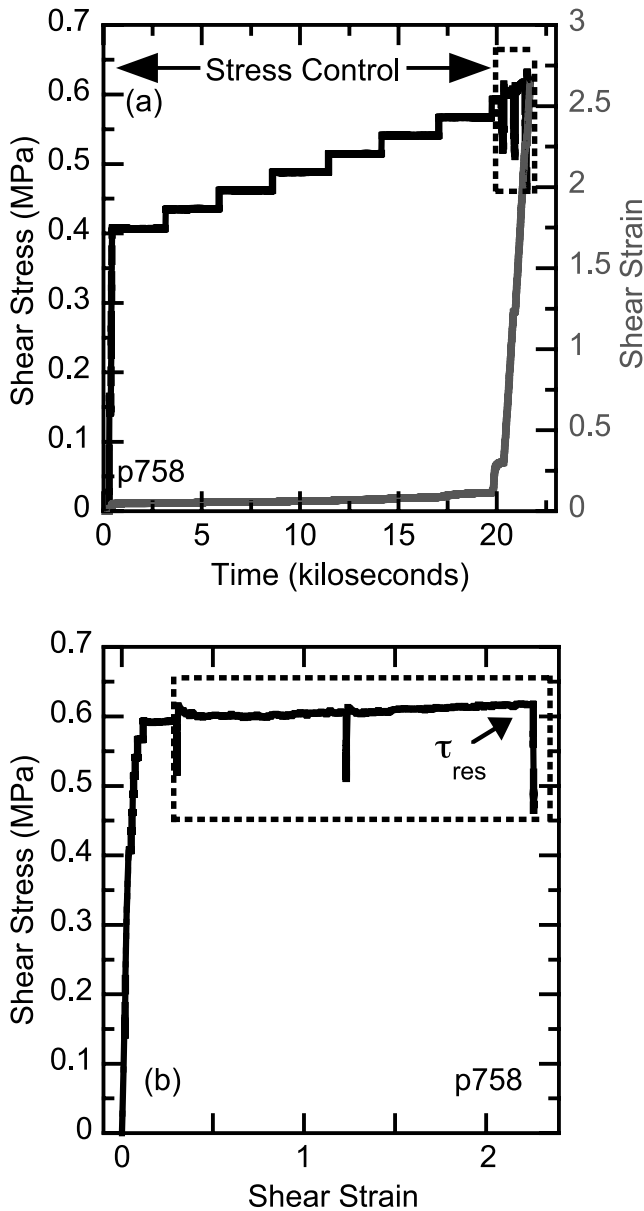
Figure 4. Shear-stress-controlled experiment without a preconditioning strain. Shear stress is incremented and the shear strain response is measured. (a) Shear stress and shear strain shown as a function of time. (b) Shear stress shown as a function of shear strain. The boxed region represents the same area in each experiment and was completed in displacement control with a 10 μm/s rate.

see Figure 3a) was observed. Each shear stress step took <2 s, during which shear strain increased linearly. When this increase was completed, shear strain rate decay commenced. Shear stress was held constant for more than 45 min at each shear stress level. The stress step increments in creep experiments were either 0.02 or 0.05 τ^* and these were held constant during a given experiment.

[26] We also investigated the effect of initial shear strain history on rheology. Shear strain is used as a proxy for fabric development. Higher initial shear strains represent more evolved shear fabric. An example of a creep experiment without initial displacement is presented in Figure 4. In these experiments, a small shear stress (<0.1 MPa) was applied in displacement control, then the experiment was switched to load control and the shear stress was quickly applied. During the initial application of shear stress, shear strain accumulated quickly. The stress-strain curves for the portion of several experiments before creep are shown in Figure 5 and indicate the consistency and experimental reproducibility that were necessary, and achieved, for these experiments. The amount of shear strain in each experiment in Figure 5 represents the total accumulated shear strain before beginning controlled stress. After the initial shear strain increment (γ_i) at a constant shearing rate, creep was induced by controlling shear stress. In cases where a steady shear strength was not reached before creep began, an average value of τ_{res}, based on an initial slip displacement of 10 mm, was used. Layer thickness for representative experiments to $\gamma_i > 1$, and all experiments at shear strain
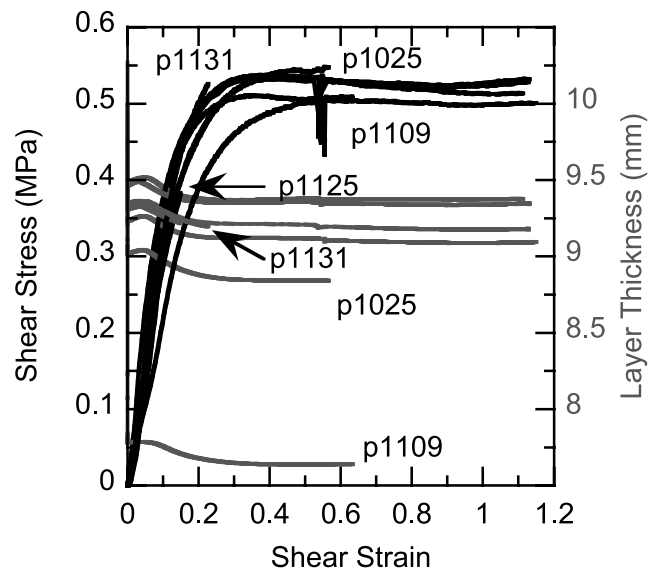
Figure 5. Stress-strain curves for initial strain of creep experiments with shear strain >0 (black curves). Shear stress becomes steady by a shear strain of 0.3 in all experiments other than p1109. Layer thickness evolves to a constant value by a shear strain of $\sim$0.3 (gray curves). Constant layer thickness corresponds to a porosity of 27%. Experiment numbers are listed at the completion of the run in before creep. Experiments to shear strain >1 are p729, p731, p732, and p737. The layer thickness trend for p1125 is hidden by other curves. Data are corrected for shear thinning [e.g., *Scott et al.*, 1994].

strain of the two control modes. In displacement control (boxed regions) the amount of shear strain is large while the time is short. In stress control the shear strain is small until tertiary creep (accelerating shear strain rate). In Figure 3a tertiary creep is observed at $\sim$20 ks, when shear strain begins to increase rapidly.

[25] After the initial "run in," we imposed a stepwise increasing shear stress. The initial shear stress applied was $\tau^* = 0.69$ (chosen because of resolution limitations at lower strain rates), with values increased incrementally until tertiary creep (indicated by a rapid increase in shear strain;
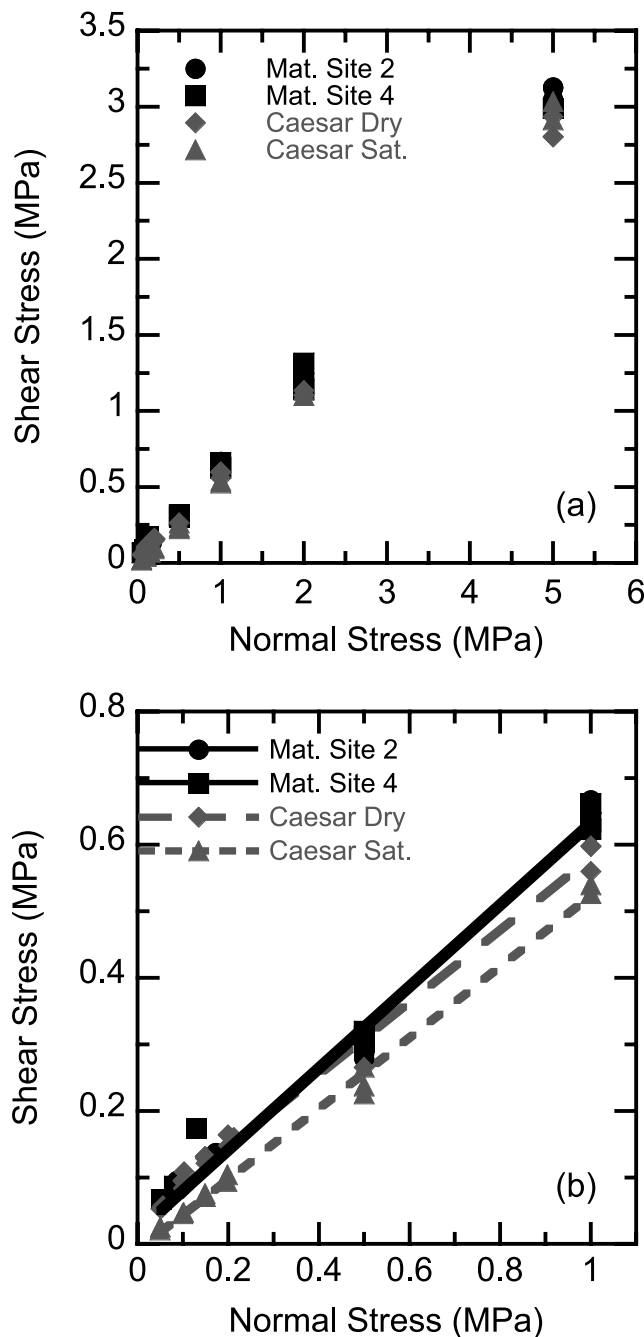
Figure 6. Coulomb failure envelop for Caesar till and two neighboring sites of Matanuska till. (a) The entire normal stress history (50 kPa to 5 MPa). (b) Low normal stress portion of the experiments. The values of cohesion (c) and internal friction angle (ϕ) are 16.6 kPa and 31.4°, respectively, for dry Matanuska till. For Caesar till, values of cohesion and internal friction angle are 29.6 kPa and 29.4° for dry samples and −6.5 kPa and 28.0° for saturated samples, respectively.

$\gamma_1 < 1$, are included in Figure 5 for reference. Porosity decreased from an initial value of 39 ± 4% to 27 ± 1% at steady state. These data show that reproducible values for the residual stress and the steady state layer thickness are

achieved by shear strain of ~0.3 indicating similar fabric development at similar shear strain.

5. Data and Observations

5.1. Shear Strength for Constant Rate of Shear Displacement

[27] The shear strength of Matanuska till (Figure 1b) generally showed a gradual evolution to steady state with increasing displacement, whereas Caesar till (Figure 1a) often showed a pronounced peak at normal stresses below 1 MPa. After the peak, shear stress weakened to a steady shear strength (Figure 1a). Peaks were most pronounced at the lowest normal stresses, becoming more gradual with increasing normal stress regardless of displacement history. Figure 1a shows peak stress at a shear strain of 0.25. For Caesar till, both air-dried and drained-saturated conditions were used. In the saturated case, larger displacements were required to obtain a residual shear strength, with most experiments showing significant strain softening. As we had less till from the Matanuska Glacier, we employed only dry experiments, lower displacements, and higher normal stresses in each experiment; therefore, it was necessary to record residual shear strength and friction at lower shear strains than for experiments on the Caesar till.

[28] Residual shear strengths were used to construct a Coulomb-Mohr failure envelope (Figure 6). Figure 6a shows residual shear strength as a function of normal stress over the entire experimental range, and Figure 6b shows the low normal stress range for all experiments. These data yield cohesion (c) and internal friction angle (ϕ) values of 16.6 kPa and 31.4° for Matanuska till and 29.6 kPa and 29.4° for Caesar till, respectively. Slight differences in grain size distributions and sample locations did not affect the residual shear strength of Matanuska till (Figure 6). Saturation caused a decrease in cohesion and internal friction angle to −6.5 kPa and 28.0°, respectively, in Caesar till. Raising normal stresses above 1 MPa, resulted in a small (~2°) increase in internal friction angle and a reduction in cohesion for Caesar till. The negative cohesion values indicate that internal friction increases with increased normal stress, which is not unusual for low normal stresses. In cases where layer thickness is not constant when corrected for shear thinning, we have not included the shear strength measurements in our regression. Repeated experiments, and experiments in which the normal stress was decreased instead of increased, showed similar values of residual shear strength. Running the normal stress increments backward resulted in little change in residual shear strength (Table 2, Figure 2). The shear strength was also calculated after creep, and second-order variations such as strain hardening or softening investigated. The comparison of the shear strength data before and after the creep experiments showed variation of <2%.

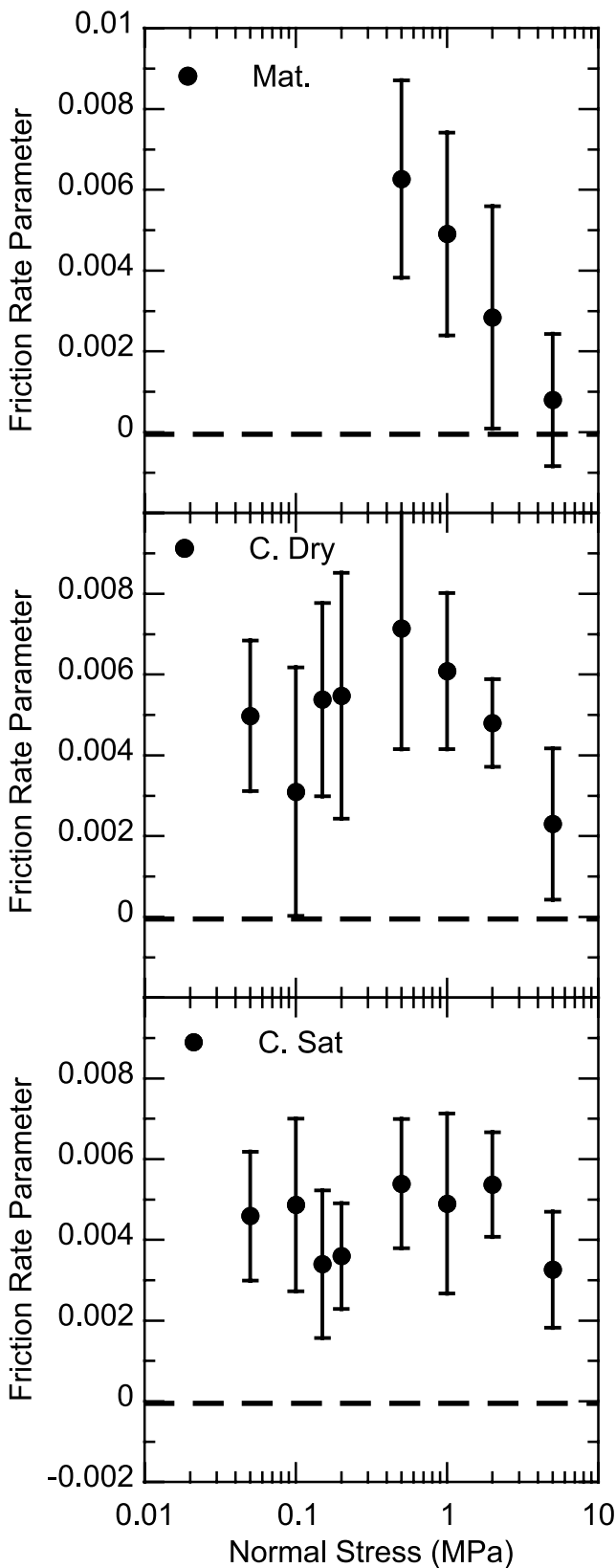### 5.2. Velocity Dependence and Frictional Constitutive Behavior

[29] The dependence of frictional strength on slip rate and slip history (e.g., memory or so-called state effects) was evaluated in the context of rate and state friction

$$\mu \equiv \mu(V, \theta) = \mu_o + a\ln\left(\frac{V}{V_o}\right) + b\ln\left(\frac{V_o\theta}{D_c}\right) \qquad (7)$$

coupled with the Dieterich aging law

$$\frac{d\theta}{dt} = 1 - \frac{V\theta}{D_c}, \qquad (8)$$

where μ is the friction coefficient, μ_0 is friction at a reference velocity (V_0), V the sliding velocity, θ a state variable representing the average lifetime of contacts during shear, and D_c the critical slip distance required to reach a new steady friction level [Dieterich, 1979, 1981; Marone, 1998; Scholz, 2002]. The constant a is termed the direct effect and represents the immediate increase in friction upon the change in velocity. The term b represents the evolution of friction to a new steady value. At steady state with $d\theta/dt = 0$, equations (5) and (6) yield the velocity dependence of friction, or friction rate parameter, $a - b$.

$$a - b = \frac{\Delta\mu_{ss}}{\Delta \ln V}. \qquad (9)$$

[30] Figure 2 inset defines the velocity and frictional terms of rate and state friction. The increase in friction at a velocity step is proportional to a times the log of the change in velocity; this is scaled by the stiffness of the testing machine. The direct friction change then decays to a new steady friction value over a characteristic slip distance, D_c. Figure 2 inset shows velocity-strengthening frictional behavior for the first two velocity steps in which the steady state friction increases with velocity. In some cases, friction exhibited strain hardening or strain softening, which transcended velocity steps. These trends presumably reflect subtle changes in fabric or till particle characteristics, and following standard practice [e.g., Marone, 1998] we removed these trends before evaluating friction rate dependence. Each increase in shearing velocity caused dilation in the layer. The displacement length of this dilation scales with the critical slip distance. Our values for the friction rate parameter were recorded at constant layer thicknesses.

[31] The velocity dependence of friction was calculated for dry Matanuska till for normal stresses of 0.5–5 MPa. For Caesar till, we determined friction velocity dependence for both saturated and dry samples. The shear strains at which friction values are taken vary because multiple normal stresses were investigated in each experiment (e.g., Figure 1). Figure 7 presents mean values of the friction rate parameter for all velocities at a given normal stress. Error bars represent one standard deviation from the mean. Till from the Matanuska Glacier showed velocity-strengthening behavior (friction rate parameter, $a - b > 0$) with the average value of the friction rate parameter decreasing steadily with increasing normal stress (Figure 7a). Under dry conditions, Caesar till displays low values of the friction

Figure 7. Friction rate parameter, $a - b$, plotted as a function of normal stress for (a) Matanuska till dry, (b) Caesar till dry, and (c) Caesar till saturated. Points are plotted as average values, with error bars at 1 standard deviation. For Figure 7a the friction rate parameter stays positive and decreases with normal stress, and data under a normal stress of 0.5 MPa are not reported because of nonsteady friction values and layer thickness. For Figure 7b, samples show velocity strengthening with the friction rate parameter value decreasing above 0.5 MPa. For Figure 7c, water saturation decreases the variability in the friction rate parameter value but does not significantly impact the average value.
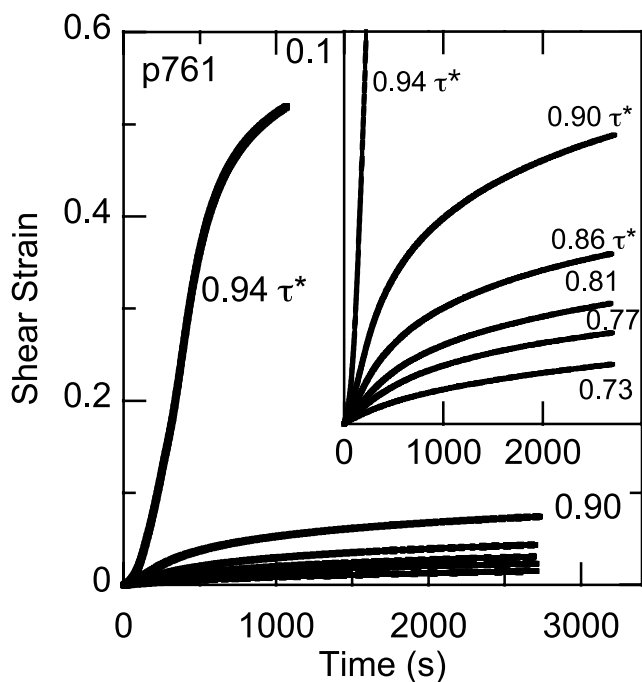
Figure 8. Shear strain history for one experiment. The inset is zoomed in to show the logarithmic decay of strain rate with time for the stable cases of $\tau^* = 0.73$ through $\tau^* = 0.90$ of the shear strength. At $\tau^* = 0.94$ of the shear strength, tertiary creep is observed, with shear strain accelerating before a transition back to primary creep.

rate parameter for normal stresses below 0.5 MPa, with the friction rate parameter exhibiting no clear dependence with normal stress below 1 MPa (Figure 7b). Saturated Caesar till yields similar velocity-strengthening results, but with ~10% lower mean values of the friction rate parameter (Figure 7c). The friction rate parameter values from postcreep tests were ~0.002 larger than those from experiments conducted in constant displacement mode throughout.

5.3. Time-Dependent Behavior

[32] In creep tests, each shear stress was held constant for 45 min, with shear strain rate determined during a 2-min window 40 min after the stress step. Stress steps began at $\tau^* \sim 0.69$; however, recording of shear strain rates $<10^{-7}\,\mathrm{s}^{-1}$ were unreliable because of noise. The typical response to a shear stress step was a jump in the shear strain rate followed by logarithmic decay of shear strain with time (Figure 8). For $\tau^* > 0.9$, tertiary (accelerating) creep was often seen (e.g., the $\tau^* = 0.94$ curve in Figure 8). Figure 8 shows the shear strain history for all shear stress steps in a representative experiment. As shear stress increased and τ^* approached unity, both the relative amount of shear strain caused by each step and the shear strain rate increased.

[33] We determined stress exponents using a simple power flow law of the form

$$\dot{\gamma} = A\tau^{*n}, \qquad (10)$$

where $\dot{\gamma}$ is shear strain rate, τ^* normalized shear stress, n stress exponent, and A is a constant that may depend on factors such as temperature, grain size, mineralogy and

effective stress, among others. This formulation differs from equation (1) in that (1) we relate the shear strain rate $\dot{\gamma}$ to the normalized shear stress τ^* (rather than the shear stress and effective pressure P_e) and (2) we assume that yield strength, $\tau_c \sim 0$. Careful analysis of the stress-strain curve in our experiments indicates that τ_c is small, with higher recording rates producing progressively smaller values. The case of small τ_c is not uncommon in soils [e.g., *Mitchell and Soga*, 2005, pp. 444–456].

[34] The value of n was 17.5 in experiments for samples with initial shear strain (γ_i) >1 (Figure 9). Samples that experienced no initial shear strain ($\gamma_i = 0$) prior to creep exhibited n of 6.8 (Figure 9). Error values for n should be assessed by experimental reproducibility; however, we do not report error values because of decreasing values of shear strain rate. For a given shear stress magnitude, the shear strain rate and corresponding stress exponent, n, varied systematically with initial (preconditioning) shear strain (Figure 9). The data show that, in general, shear strain rates decrease and stress exponent values increase with increasing initial shear strain (Figure 9).

[35] In addition to the main set of creep experiments conducted at 1 MPa normal stress, suites of creep tests were conducted at 0.5 and 5 MPa (Table 2; Figure 10). These data show that normal stress did not have a significant impact on shear strain rate or n (Figure 10). Creep experiments at 0.5 and 5 MPa normal stress with $\gamma_i \sim 0$ exhibit a smaller shear strain rate than experiments conducted at 1 MPa normal stress. This variation is consistent with experimental reproducibility at 1 MPa normal stress. Increasing γ_i to ~ 1 resulted in lower shear strain rate and increased n for both normal stresses (Figure 10).
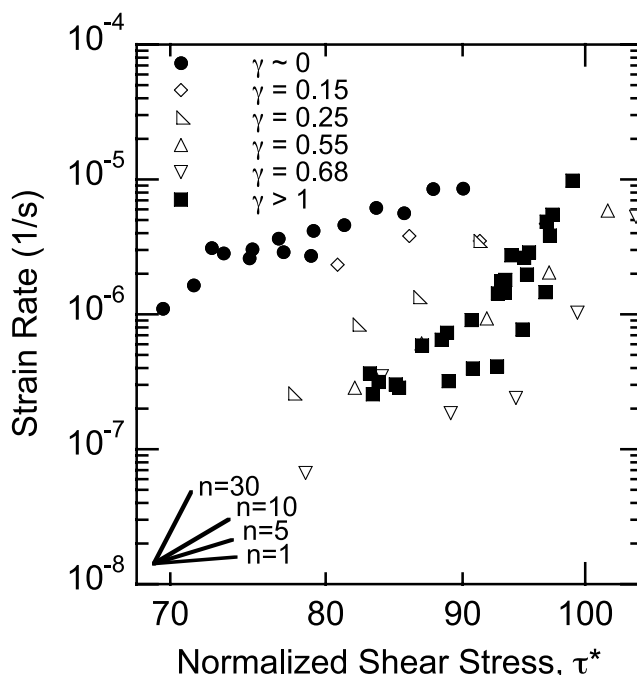
Figure 9. Shear strain rate plotted as a function of the normalized shear stress. All data represent a normal stress of 1 MPa. Fiducial curves correspond to the trend of $n = 1, 5,$ 10, and 30. Best fit regression gives n values of 6.8 at 40 min after a shear stress step at $\gamma_i \sim 0$ and 17.5 at $\gamma_i > 1$.
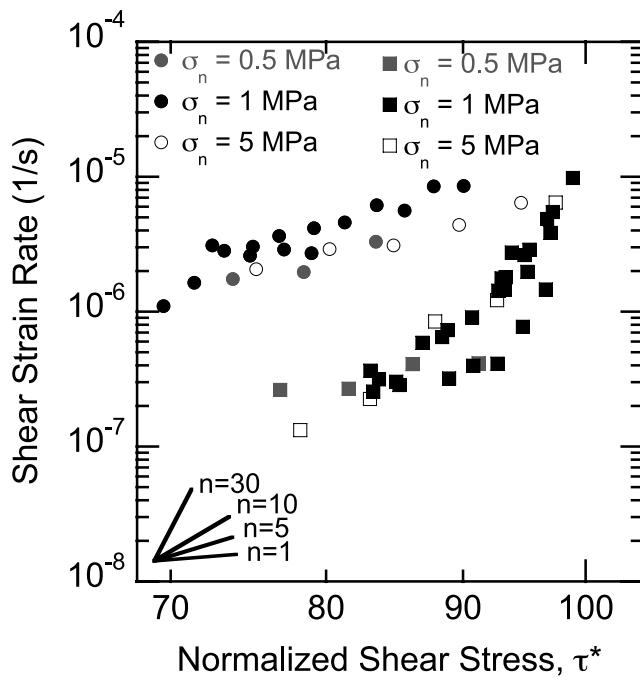
Figure 10. Shear strain rate plotted as a function of the normalized shear stress for normal stress of 0.5, 1, and 5 MPa. Circles and squares represent $\gamma_i \sim 0$ and $\gamma_i \sim 1$, respectively.

[36] Generally, the onset of tertiary creep began at lower values of τ^* for experiments with smaller γ_i. For experiments with $\gamma_i = 0$, tertiary creep occurred at all shear stresses greater than 0.9 τ^*. For $\gamma_i \geq 1$, tertiary creep did not occur until $\tau^* \geq 1$. Note that shear stress can exceed τ_{res} because of healing and other second-order friction effects.

[37] The accumulation of shear strain is many times larger during tertiary creep than in logarithmic creep. In a few cases, we observed a transition from tertiary creep back to logarithmic decay of shear strain rate (Figure 8). The final stress step to $\tau^* = 0.94$ (Figure 8) shows such a case of transiently accelerating creep. After a sample exhibited tertiary creep, all subsequent shear stress increases showed acceleration, even if the material had strengthened and transitioned back to a logarithmic decay in shear strain rate. Thus, after tertiary creep occurred we ceased creep tests, and data associated with tertiary creep are not considered in calculations of stress exponents.

6. Discussion

6.1. Coulomb Plastic Failure

[38] Our data are well represented by a linear Coulomb failure envelope, with a small rate dependence of shear strength. Residual shear strength for both Matanuska and Caesar till increased linearly with normal stress, with cohesion near zero. Saturation reduced the residual shear strength and cohesion values. The small, positive, friction rate parameter values show that tills studied under these conditions are not perfectly Coulomb plastic. However, the small dependence of friction and strength on velocity does allow for the Coulomb plastic generalization for many purposes [*Kamb*, 1991; *Iverson et al.*, 1998; *Tulaczyk et*

al., 2000]. Casting friction values in terms of equation (10) yields $n > 60$ in all experiments, justifying a plastic approximation. When analyzed in terms of equation (3) these data correspond to B values of ~ 0.004 to ~ 0.01, comparable to previous studies of till and soils [e.g., *Iverson et al.*, 1998; *Tulaczyk et al.*, 2000; *Mitchell and Soga*, 2005].

[39] We observe large stress exponents ($n > 10$), indicating nearly Coulomb plastic deformation, in creep experiments when an inferred fabric was present and/or when τ^* exceeded 0.90 (Figure 9). Increasing shear strain is generally observed to lead to shear fabric development within sheared granular and clay-rich materials [e.g., *Logan et al.*, 1979], so we infer that high stress or fabric development favors Coulomb plastic behavior. At $\gamma_i > 0.15$, shear strain rate decreases with increased shear strain while stress sensitivity increases, indicating a transition to more plastic deformation. Once a γ_i of ~ 1 was attained, the sensitivity of shear strain rate to accumulated shear strain saturated, and no further decrease in shear strain rate was observed with increasing shear strain. We infer that a relatively steady fabric was achieved for shear strain of approximately 1. The progression of till fabrics observed in this study is consistent with studies of till micromorphology [e.g., *Thomason and Iverson*, 2006; *Larsen et al.*, 2006; *Iverson et al.*, 2008]. In our experiments, rheology did not vary significantly above shear strain of 1; however, it is possible that grains are rotating and becoming aligned at higher shear strain. We did not conduct detailed fabric analysis to analyze fabric at higher shear strains.

[40] For shear stress levels above 0.90 τ^*, tertiary creep and high stress exponent behavior are observed in samples with $\gamma_i = 0$. In experiments with $\gamma_i \sim 1$, tertiary creep was not observed until higher shear stresses. Grain rearrangement and shear compaction in high shear strain experiments may have led to a slight strengthening in the till layers, keeping these experiments from showing tertiary creep over the timescale of our steps. In creep experiments, tertiary creep is not expected at low shear stress [e.g., *Mitchell and Soga*, 2005]. It is possible that holding shear stress longer at a given level could lead to grain reorientation into weaker positions producing tertiary creep at our highest stresses [*Feda*, 1992; *Mitchell and Soga*, 2005]; however, this is beyond the scope of the present study.

6.2. Rate and State Friction

[41] In addition to calculating the friction rate parameter with equation (7), we developed simple forward and inverse models of the rate and state friction. In order to calculate accurate values for the rate and state parameters a, b, and D_c, machine and sample stiffness must be taken into account [*Marone et al.*, 1990]. The machine stiffness is known from calibrations; to get the effective stiffness of the machine with sample assembly, we used the initial slope of the friction displacement curve at step increases in load point velocity. The positive rate dependence of friction for a jump in driving velocity, characterized by the friction parameter a, produces a linear elastic stress increase that is a measure of effective system stiffness In our experiments, this stiffness (when normalized by the applied normal stress) was 0.005 μm^{-1} at a normal stress of 1 MPa.

[42] For Matanuska till, the decrease in friction rate parameter with increasing normal stress (Figure 7) is caused by a decrease in a with increasing normal stress. Values of a fell from ~0.01 at 0.5 MPa to 0.0075, 0.0070, and 0.0065 at stresses of 1, 2, and 5 MPa, respectively. Values of b remained relatively consistent near 0.004. Values of D_c varied considerably and were difficult to assess. Data under 0.5 MPa are not presented for Matanuska till because of unsteady friction levels and layer thickness in our displacement range. Dry Caesar till showed consistent a values of 0.007–0.01 and b values of 0.004–0.006. Saturation elevated values of both a and b. Values of a ranged from 0.008 to 0.01, with corresponding larger b of 0.005 yielding the friction rate parameter shown in Figure 7. These data are consistent with reported values of the friction rate parameter, in which values are slightly positive or negative in glacial till [*Tika et al.*, 1996; *Iverson et al.*, 1998] and fault gouge [e.g., *Marone et al.*, 1990; *Marone*, 1998, *Scholz*, 2002].

6.3. Pseudoviscous Deformation During Nonsteady Creep

[43] We use the term pseudoviscous to describe deformation for which shear stress is nearly linearly related to shear strain (e.g., Newtonian). Our results are consistent with previous studies of polymineralic granular and clay-rich materials showing that inelastic yielding (creep) begins at very low resolved shear stress [*Bishop*, 1966; *Karner and Marone*, 2001; *Mitchell and Soga*, 2005]. Our data indicate a stress exponent of 6.8 for tills with no initial shear fabric and stresses below 0.9 τ^* when determined on the basis of data collected 40 min after stress steps using equation (10). For comparison, the value of n is 9.0 when determined from shear strain rate 20 min after the shear stress step. Because shear strain rate continues to decay with time following a shear stress increase, the value of n likely continues to decrease. Experiments at $\gamma_i > 1$, show larger values of n than experiments at $\gamma_i \sim 0$.

[44] The experiments of *Ho et al.* [1996] showed smaller, more nearly linear-viscous, values of n for Batestown till, with the strain rate still decreasing after 24 h. These variations in n indicate that true secondary creep (constant shear strain rate) was not attained in those experiments. Previous work has indicated that true secondary creep may not be possible during frictional shear of a granular layer, due to continuous formation and breaking of adhesive contact bonds and grain rearrangement throughout deformation [e.g., *Feda*, 1992; *Mitchell and Soga*, 2005, section 12.3]. Thus, the reported values of n in this study represent maximum values of the power law stress exponent, and should be used with care.

6.4. Recovery

[45] As discussed earlier, a small recovery of the shear strength was seen in many cases during tertiary creep, leading to a transition back to logarithmically decaying shear strain rate. In all cases of a transition from tertiary creep, the slip velocity was <1000 μm/s, which is well within the capabilities of the testing apparatus, indicating that the strengthening was not a machine artifact. Similar behavior was seen in the normal stress reduction experiments done by *Moore and Iverson* [2002]. In both cases, the recovery of the sample is thought to be the result of material conditions, not apparatus effects. *Moore and Iverson* [2002] showed that this transition correlated with nonsteady pore pressure created by layer thickness variations during shear.

[46] In our experiments, the slight strengthening within the layer and transition from tertiary to logarithmic creep was seen under both dry and water-saturated conditions. This implies that localized pore pressure oscillations and feedbacks could not have produced the material strengthening in at least some of our experiments. Additionally, the change in layer thickness with shear strain became slightly more negative than in other portions of the experiment during the transition from tertiary to logarithmic creep in some, but not all, experiments. This change in slope represents a slight compaction or a decrease in dilatancy.

6.5. Normal Stress Independence of Rheology

[47] In both controlled shear velocity and shear stress experiments, changing normal stress did not change the observed rheology. Velocity dependence of friction did have slight variations with normal stress from 50 kPa to 5 MPa (Figures 4a and 4b); however, the small change of the friction rate parameter corresponds to a large n and nearly Coulomb plastic rheology. Results of creep experiments at 0.5, 1, and 5 MPa show nearly identical shear strain rates and n values (Figure 10). These data imply that rheology at stresses relevant in glacial settings is relatively insensitive to normal stress within the range tested.

7. Conclusions

[48] Our experiments show that till behaves as a nearly plastic material at its shear strength and as a power law creep material (nearly viscous) at stresses below 90% of the residual shear strength and at shear strains much lower than 1. The power law stress exponent n increases systematically with initial shear strain and fabric development in sheared till. We hypothesize that the transition from pseudoviscous to plastic behavior, which occurs with increasing shear stress, is due to shear localization and formation of one or more discrete shear bands within the layer. This hypothesis will be tested further in future experiments. During tertiary creep at or near the shear strength, acceleration occurred with essentially plastic deformation taking place. Controlling the shear rate and keeping till at its shear strength shows plastic deformation with little stress dependence on the shear strain rate. This is represented by a slight velocity-strengthening trend corresponding, to $n > 60$.

[49] The results of this study imply that a viscous or pseudoviscous process could take place within basal till of a glacier prior to the onset of plastic deformation [*Alley*, 2000]. In cases where slow relative strains are occurring within the bed of a glacier, the shear stress applied may be lower than the shear strength of the bed. In this case, slow pseudoviscous creep could occur. If the shear stress on the bed is near or larger than the shear strength of the underlying bed, a plastic model of deformation seems likely. The initial viscous or pseudoviscous behavior only occurs at low strains of order 1 or less. Permeability and consolidation state complicates the natural system. In cases where pore pressure diffusion is slow (e.g., sufficiently impermeable till), a dilatant-hardening system could preclude viscous

deformation [e.g., *Moore and Iverson*, 2002]. Our results suggest that once significant strain occurs within the bed, some mechanism, such as, ice quakes, ploughing, etc., would be needed to destroy the effects of shear strain for the possibility of viscous deformation, but these hypotheses need to be tested. Regulation processes such as dilatant hardening could control deformation even if shear fabric is destroyed.

References

Alley, R. B. (2000), Continuity comes first: Recent progress in understanding subglacial deformation, in *Deformation of Glacial Materials, Geol. Soc. London Spec. Publ. Ser.*, vol. 176, edited by A. J. Maltman, B. Hubbard, and M. J. Hambrey, pp. 171–179, Geol Soc of London, London.

Alley, R. B., D. D. Blankenship, C. R. Bentley, and S. T. Rooney (1986), Deformation of till beneath Ice Stream B, West Antarctica, *Nature*, 322, 57–59, doi:10.1038/322057a0.

Alley, R. B., D. D. Blankenship, S. T. Rooney, and C. R. Bentley (1989a), Water-pressure coupling of sliding and bed deformation: part I. Water system, *J. Glaciol.*, 35(119), 108–118.

Alley, R. B., D. D. Blankenship, S. T. Rooney, and C. R. Bentley (1989b), Water-pressure coupling of sliding and bed deformation: part II. Velocity-depth profiles, *J. Glaciol.*, 35(119), 119–129.

Anandakrishnan, S., and C. R. Bentley (1993), Micro-earthquakes beneath Ice Streams B and C, West Antarctica: Observations and implications, *J. Glaciol.*, 39(133), 455–462.

Anthony, J. L., and C. Marone (2005), Influence of particle characteristics on granular friction, *J. Geophys. Res.*, 110, B08409, doi:10.1029/2004JB003399.

Bird, P. (1984), Hydration-phase diagrams and friction of montmorillonite under laboratory and geologic conditions, with implications for shale compaction, slope stability, and strength of fault gouge, *Tectonophysics*, 107, 235–260, doi:10.1016/0040-1951(84)90253-1.

Bishop, A. W. (1966), The strength of soils as engineering materials, *Geotechnique*, 2(1), 89–130.

Blankenship, D. D., C. R. Bentley, S. T. Rooney, and R. B. Alley (1986), Seismic measurements reveal a saturated porous layer beneath an active Antarctic ice stream, *Nature*, 322, 54–57, doi:10.1038/322054a0.

Boulton, G. S., and R. C. A. Hindmarsh (1987), Sediment deformation beneath glaciers: Rheology and geological consequences, *J. Geophys. Res.*, 92(B9), 9059–9082, doi:10.1029/JB092iB09p09059.

Brace, W. F., and J. D. Byerlee (1966), Stick-slip as a mechanism for earthquakes, *Science*, 153(3739), 990–992, doi:10.1126/science.153.3739.990.

Brown, K. M., A. Kopf, M. B. Underwood, and J. L. Weinberger (2003), Compositional and fluid pressure controls on the state of stress on the Nankai subduction thrust: A weak plate boundary, *Earth Planet. Sci. Lett.*, 214, 589–603, doi:10.1016/S0012-821X(03)00388-1.

Clarke, G. K. C. (2005), Subglacial processes, *Annu. Rev. Earth Planet. Sci.*, 33, 247–276, doi:10.1146/annurev.earth.33.092203.122621.

Coulomb, C. A. (1781), Théorie des machines simples, en ayant égard au frotement de leurs parties, et a la roideur des cordages, *Mem. Math. Phys.*, X, 161–342.

Dieterich, J. H. (1979), Modeling of rock friction: 1. Experimental results and constitutive equations, *J. Geophys. Res.*, 84(B5), 2161–2168, doi:10.1029/JB084iB05p02161.

Dieterich, J. H. (1981), Constitutive properties of faults with simulated gouge, in *Mechanical Behavior of Crustal Rocks:The Handin Volume, Geophys. Monogr. Ser.*, vol. 24, edited by N. L. Carter et al., pp. 103–120, AGU, Washington, D. C.

Ekstrom, G., M. Nettles, and G. A. Abers (2003), Glacial earthquakes, *Science*, 302(5645), 622–624, doi:10.1126/science.1088057.

Ekstrom, G., M. Nettles, and V. C. Tsai (2006), Seasonality and increasing frequency of Greenland glacial earthquakes, *Science*, 311(5768), 1756–1758, doi:10.1126/science.1122112.

Engelhardt, H., and B. Kamb (1997), Basal hydraulic system of a West Antarctic ice stream: Constraints from borehole observations, *J. Glaciol.*, 43(144), 207–230.

Engelhardt, H., and B. Kamb (1998), Basal sliding of Ice Stream B, West Antarctica, *J. Glaciol.*, 44(147), 223–230.

Engelhardt, H., N. Humphery, B. Kamb, and M. Fahnstock (1990), Physical conditions at the base of a fast moving Antarctic ice stream, *Science*, 248(4951), 57–59, doi:10.1126/science.248.4951.57.

Feda, J. (1992), *Creep of Soils and Related Phenomena*, Elsevier, Amsterdam.

Fowler, A. C. (2003), On the rheology of till, *Ann. Glaciol.*, 37(1), 55–59, doi:10.3189/172756403781815951.

Frye, K. M., and C. Marone (2002), Effect of humidity on granular friction at room temperature, *J. Geophys. Res.*, 107(B11), 2309, doi:10.1029/2001JB000654.

Haefner, R. J. (Ed.) (1999), A conference on fractured glacial tills: Field trip guide to selected fractured glacial till sites and soils in central Ohio, paper presented at Water Management Association of Ohio Spring Conference on Fractured Glacial Tills, U. S. Geol. Surv., Columbus, Ohio, 10 May 1999.

Hindmarsh, R. C. A. (1997), Deforming beds: Viscous and plastic scales of deformation, *Quat. Sci. Rev.*, 16, 1039–1056, doi:10.1016/S0277-3791(97)00035-8.

Ho, C. L., J. C. Vela, J. W. Jenson, and P. U. Clark (1996), Evaluation of long-term time-rate parameters of subglacial till, in *Measuring And Modeling Time-Dependent Soil Behavior, Am. Soc. Civ. Eng. Spec. Publ. Ser.*, vol. 61, edited by T. C. Sheahan and V. N. Kaliakin, pp. 122–136, Am. Soc. of Civ. Eng., Reston, Va.

Hooke, R., B. Le, B. Hanson, N. R. Iverson, P. Jansson, and U. H. Fischer (1997), Rheology of till beneath Storglaciaren, Sweden, *J. Glaciol.*, 43(143), 172–179.

Ikari, M. J., D. M. Saffer, and C. Marone (2007), Effect of hydration state on the frictional properties of montmorillonite-based fault gouge, *J. Geophys. Res.*, 112, B06423, doi:10.1029/2006JB004748.

Iverson, N. R., R. W. Baker, and T. S. Hooyer (1997), A ring-shear device for the study of till deformation: Tests on tills with contrasting clay contents, *Quat. Sci. Rev.*, 16(9), 1057–1066, doi:10.1016/S0277-3791(97)00036-X.

Iverson, N. R., T. S. Hooyer, and R. W. Baker (1998), Ring-shear studies of till deformation: Coulomb-plastic behavior and distributed strain in glacier beds, *J. Glaciol.*, 44(148), 634–642.

Iverson, N. R., D. Cohen, T. S. Hooyer, U. H. Fischer, M. Jackson, P. L. Moore, G. Lappegard, and J. Kohler (2003), Effects of basal debris on glacier flow, *Science*, 301, 81–84, doi:10.1126/science.1083086.

Iverson, N. R., T. S. Hooyer, J. F. Thomason, M. Graesch, and J. R. Shumway (2008), The experimental basis for interpreting particle and magnetic fabrics of sheared till, *Earth Surf. Processes Landforms*, 33, 627–645.

Jenson, J. W., P. D. Clark, D. R. MacAyeal, C. Ho, and J. C. Vela (1995), Numerical modeling of advective transport of saturated deformaing sediment beneath the Lake Michigan Lobe, Laurentide Ice Sheet, *Geomorphology*, 14(2), 157–166, doi:10.1016/0169-555X(95)00056-0.

Kamb, B. (1991), Rheological nonlinearity and flow instability in the deforming bed mechanism of ice stream motion, *J. Geophys. Res.*, 96(B10), 16,585–16,595, doi:10.1029/91JB00946.

Kamb, B. (2001), Basal zone of the West Antarctic ice streams and its role in lubrication of their rapid motion, in *The West Antarctic Ice Sheet*, edited by R. B. Alley and R. A. Bindschadler, pp. 99–157, AGU, Washington, D. C.

Karner, S. L., and C. Marone (2001), Frictional restrengthening in simulated fault gouge: Effect of shear load perturbations, *J. Geophys. Res.*, 106(B9), 19,319–19,337, doi:10.1029/2001JB000263.

Kavanaugh, J. L., and G. K. C. Clarke (2006), Discrimination of the flow law for subglacial sediment using in situ measurements and an interpretation model, *J. Geophys. Res.*, 111, F01002, doi:10.1029/2005JF000346.

Knuth, M. C., and C. Marone (2007), Friction of sheared granular layers: Role of particle dimensionality, surface roughness, and material properties, *Geochem. Geophys. Geosyst.*, 8, Q03012, doi:10.1029/2006GC001327.

Larsen, N. K., J. A. Piotrowski, and F. Christiansen (2006), Microstructures and microshears as a proxy for strain in subglacial diamicts: Implications for basal till formation, *Geology*, 34(10), 889–902, doi:10.1130/G22629.1.

Logan, J. M., and K. A. Rauenzahn (1987), Frictional dependence of gouge mixtures of quartz and montmorillonite on velocity, composition, and fabric, *Tectonophysics*, 144, 87–108, doi:10.1016/0040-1951(87)90010-2.

Logan, J. M., M. Friedman, N. Higgs, C. Dengo, and T. Shimamodo (1979), Experimental studies of simulated fault gouges and their application to studies of natural fault zones, in *Analysis of Actual Fault Zones in Bedrock, U.S. Geol. Surv. Open File Rep. 1239*, pp. 305–343, U.S. Geol. Surv., Reston, Va.

Mair, K., and C. Marone (1999), Friction of simulated fault gouge for a wide range of velocities and normal stress, *J. Geophys. Res.*, 104(B12), 28899–28,914, doi:10.1029/1999JB900279.

Marone, C. (1998), Laboratory-derived friction constitutive laws and their application to seismic faulting, *Annu. Rev. Earth Planet. Sci.*, 26, 643–696, doi:10.1146/annurev.earth.26.1.643.

Marone, C., and B. Kilgore (1993), Scaling of the critical slip distance for seismic faulting with shear strain in fault zones, *Nature*, *362*, 618–621, doi:10.1038/362618a0.

Marone, C., C. B. Raleigh, and C. H. Scholz (1990), Frictional behavior and constitutive modeling of simulated fault gouge, *J. Geophys. Res.*, *95*(B5), 7007–7025, doi:10.1029/JB095iB05p07007.

Mitchell, J. K., and K. Soga (2005), *Fundamentals of Soil Behavior*, 3rd ed., John Wiley, Hoboken, N. J.

Moore, P. L., and N. R. Iverson (2002), Slow episodic shear of granular materials regulated by dilantant strengthening, *Geology*, *30*(9), 843–846, doi:10.1130/0091-7613(2002)030<0843:SESOGM>2.0.CO;2.

Paterson, W. S. B. (1994), *The Physics of Glaciers*, 3rd ed., Butterworth-Heinemann, Oxford, U.K.

Peters, L. E., S. Anandakrishnan, R. B. Alley, J. P. Winberry, D. E. Voight, A. M. Smith, and D. L. Morse (2006), Subglacial sediments as a control on the onset and localization of two Siple Coast ice streams, West Antarctica, *J. Geophys. Res.*, *111*, B01302, doi:10.1029/2005JB003766.

Ruina, A. (1983), Slip instability and state variable friction laws, *J. Geophys. Res.*, *88*(B12), 10,359–10,370, doi:10.1029/JB088iB12p10359.

Scholz, C. H. (2002), *The Mechanics of Earthquakes and Faulting*, 2nd ed., Cambridge Univ. Press, Cambridge, U.K.

Scott, D., C. Marone, and C. Sammis (1994), The apparent friction of granular fault gouge in sheared layers, *J. Geophys. Res.*, *99*(B4), 7231–7247, doi:10.1029/93JB03361.

Skempton, A. W. (1985), Residual strength of clays in landslides, folded strata, and the laboratory, *Geotechnique*, *35*(1), 3–18.

Thomason, J. F., and N. R. Iverson (2006), Microfabric and microshear evolution in deformed till, *Quat. Sci. Rev.*, *25*, 1027–1038, doi:10.1016/j.quascirev.2005.09.006.

Tika, T. E., P. R. Vaughan, and L. Lemos (1996), Fast shearing of pre-existing shear zones in soil, *Geotechnique*, *46*(22), 197–233.

Truffer, M., W. D. Harrison, and K. A. Echelmeyer (2000), Glacier motion dominated by processes deep in underlying till, *J. Glaciol.*, *45*, 495–505.

Tulaczyk, S. (2006), Scale independence of till rheology, *J. Glaciol.*, *52*(178), 377–380, doi:10.3189/172756506781828601.

Tulaczyk, S., W. B. Kamb, and H. F. Engelhardt (2000), Basal mechanics of Ice Stream B, West Antarctica: 1. Till mechanics, *J. Geophys. Res.*, *105*(B1), 463–481, doi:10.1029/1999JB900329.

———————————

R. B. Alley, S. Anandakrishnan, C. Marone, and A. P. Rathbun, Rock and Sediment Mechanics Laboratory and Pennsylvania State Ice and Climate Research, Department of Geosciences, Pennsylvania State University, University Park, PA 16802, USA. (ralley@geosc.psu.edu; sak@geosc.psu.edu; cjm@geosc.psu.edu; arathbun@geosc.psu.edu)